
Channel-Oriented Design for EEG-to-Music Reconstruction

Jiabin Qing
UC Berkeley

Junwei Lu
Harvard University

Lexin Li
UC Berkeley

Abstract

Brain-computer interfaces aim to decode naturalistic stimuli from neural signals, yet most progress to date has focused on vision and language. In this article, we study a more challenging but far less explored setting, EEG-to-music reconstruction, where signals are weak, distributed, and highly susceptible to noise and channel variability. Our central finding is that early channel mixing destroys weak but discriminative EEG signals. To address this, we propose a channel-oriented design with three key components. Specifically, channel-wise tokenization treats each electrode as an explicit token to retain spatially localized neural evidence, channel-wise multi-view self-distillation enforces consistency across temporal crops and random channel subsets to learn robust and distributed representations, and channel-wise data augmentation introduces structured channel dropout to improve invariance to noise, artifacts, and missing electrodes. Together, these components preserve weak yet informative signals across channels and enable stable alignment to a semantic music representation space. We integrate this channel-oriented design within an encoding-alignment-decoding pipeline for EEG-to-music reconstruction. Theoretically, we characterize when preserving channel-level structure leads to improved alignment. Empirically, we compare with a range of state-of-the-art baselines and demonstrate consistent and significant performance gains. Codes are available at <https://github.com/jqin4749/EEG-to-Music>.

1 Introduction

Brain-computer interfaces (BCIs) aim to decode naturalistic stimuli from neural activities measured by techniques such as functional magnetic resonance imaging (fMRI) and electroencephalography (EEG), providing a pathway toward understanding perception and enabling new forms of human-machine interaction. Recent advances, mostly driven by deep learning and generative models, have led to impressive progress in reconstructing visual and linguistic content from brain signals [22, 21, 25, 5, 24].

In this article, we study EEG-to-music reconstruction, i.e., recovering semantically faithful music from noninvasive EEG signals recorded while a subject listens to naturalistic songs. This setting is far less explored than vision or language reconstruction, and is especially challenging, because music is continuous, temporally structured, and semantically rich, involving rhythm, melody, timbre, and emotion, whereas EEG signals are weak, distributed across electrodes, and highly sensitive to artifacts and channel variability. Critically, music-related information is not localized to a single region but is encoded as subtle patterns spread across many channels, each providing a partial and noisy view of the underlying neural activity. To date, only limited work has studied EEG-to-music reconstruction [11, 15, 18].

Despite these challenges, existing approaches largely adopt standard deep learning pipelines that mix channels early, either through convolution, pooling, or block-wise tokenization. While such designs are useful in other domains, they are poorly suited for EEG-to-music reconstruction. Early channel mixing entangles signal with channel-specific noise, obscures the spatial origin of neural evidence, and dilutes discriminative patterns that are only visible across a set of weak electrodes. As a result, current music reconstruction is often ineffective.

Our central observation is that a key bottleneck in EEG-to-music reconstruction lies in representation learning rather than decoding: prematurely mixing channels obscures the signals needed for downstream alignment and generation. This motivates us to adopt and develop a new design principle, channel orientation, where the goal is not to avoid cross-channel interactions, but instead to preserve electrode-level structure and defer channel integration to later stages where it can be learned adaptively. We instantiate this principle through three complementary components. First, channel-wise tokenization treats each electrode as an explicit token, preserving spatially localized neural evidence and allowing the model to learn cross-channel relationships without losing channel identity. Second, channel-wise multi-view self-distillation enforces consistency across temporal crops and random channel subsets, encouraging the model to capture distributed and stable neural patterns while remaining robust to partial observations. Third, channel-wise data augmentation, implemented via structured channel dropout, improves invariance to noise, artifacts, and missing electrodes by forcing the model to infer consistent representations from varying channel configurations. Together, these components enable the model to retain weak but informative signals distributed across channels, and to build a robust representation suitable for downstream reconstruction.

We integrate the channel-oriented design within an encoding-alignment-decoding pipeline, further incorporating a pretrained CLAP music encoder, a standard CLIP-style contrastive learning alignment, and a pretrained diffusion model, for EEG-to-music reconstruction. We evaluate our method both theoretically and empirically. We summarize our main contributions as follows.

- A representation-centric perspective for EEG-based music reconstruction: We identify premature channel mixing as a main failure mode in existing EEG pipelines, and recast EEG-to-music reconstruction as a problem of preserving and aligning channel-level neural signals before generation. This perspective shifts the focus from decoder capacity to representation design, and our results support the central claim that representation design, not only generative decoder capacity, is crucial for EEG decoding of naturalistic stimuli.
- A unified channel-oriented framework for EEG representation learning: We develop a coherent design that integrates channel-wise tokenization, multi-view self-distillation, and structured channel-level augmentation. These components act jointly to enforce consistency under varying channel subsets and temporal resolutions, while still allowing adaptive cross-channel aggregation, and producing stable EEG representations for music alignment.
- Theoretical analysis and understanding of the proposed design: We analyze channel masking through the induced augmentation graph and show that, under some reasonable conditions, channel-wise masking yields strictly smaller normalized cross-cluster overlap than block masking. This result characterizes when preserving channel-level structure leads to improved alignment.
- Strong empirical validation and comparisons: We perform systematic comparisons against EEG2Mel, the primary existing EEG-to-music solution, as well as multiple state-of-the-art EEG foundation models within a unified reconstruction pipeline. Our method achieves the best performance on semantic and embedding-level metrics, including a CLAP score of 0.683 and a 50-way identification accuracy of 0.487, improving over the strongest baselines by significant margins. Ablation studies further confirm that each component contributes meaningfully to the final performance.
- Improved interpretability: By preserving channel-level representations, our approach enables direct inspection of per-channel contributions via attention weights. The resulting channel attention patterns reveal anatomical and stimulus-specific structures, such as temporal-region dominance consistent with auditory processing, and capture higher-level effects such as cultural familiarity. This provides a level of interpretability that is typically absent in blackbox EEG foundation models.

2 Related Work

Brain Decoding. Brain decoding has advanced rapidly in vision and language [22, 21, 25, 5, 24]. In vision, [24] maps fMRI signals into the latent space of Stable Diffusion, while [21] employs CLIP-style contrastive learning to align fMRI with image representations. For EEG-based image decoding, [22] also adopts CLIP-based alignment. A smaller body of work focuses on pretraining EEG encoders prior to alignment, including [4] and [2]. Our work follows this encoder-first paradigm, but investigates whether it can support a continuous music target from EEG, whose perceptual content depends on temporal structure as well as high level semantics.

EEG-to-Music Reconstruction. Early work by [11, 15] introduces naturalistic music EEG datasets and studies neural responses to music through correlation-based analyses. EEG2Mel [18], the closest reconstruction method to ours, maps EEG directly to mel spectrograms and then reconstructs audio from those spectra. This makes spectrogram prediction the central learning target. In contrast, we learn

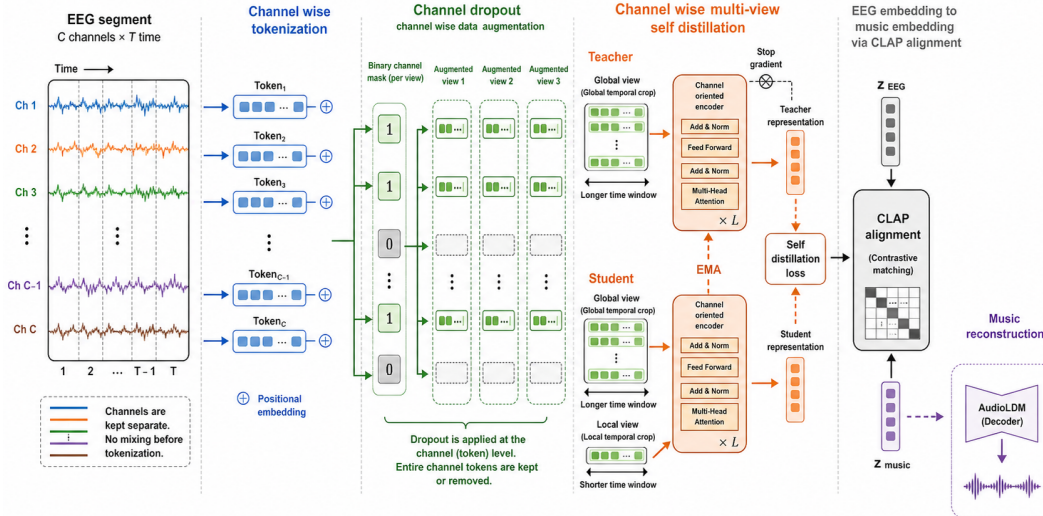


Figure 1: Overview of the pipeline architecture. Each channel is tokenized separately, and random channel subsets are dropped during training. Local views are short temporal crops, while global views are long temporal crops. The student receives both view types, the teacher receives only global views, and the objective matches their representations of the same segment.

an explicit EEG-music alignment space and apply a pretrained audio generator only after alignment, enabling us to assess whether the EEG representation captures semantic musical information rather than merely local spectrogram similarity.

EEG Encoders. Recent transformer-based EEG encoders learn general neural representations from large-scale datasets [6, 10, 30, 26–29], but are often evaluated on classification tasks rather than high-level stimulus reconstruction. While these models provide useful EEG priors, they do not explicitly preserve electrode identity throughout the full pipeline from pretraining to music alignment. For instance, LaBraM [10] uses per-channel tokens with masked prediction over a learned neural codebook, whereas EEG DINO [30] adopts a multi-view self-supervised framework with spatial patch tokens that group neighboring channels, making it the closest baseline for our block-tokenization comparison. EEGPT [26] and CBraMod [27] incorporate architectural components such as convolutional stems or criss-cross attention that mix information across dimensions. In contrast, we treat channel orientation as a design constraint across tokenization, self-distillation, and alignment augmentation, and evaluate its effect in EEG-to-music reconstruction.

3 Channel Oriented Design

Our EEG-to-music pipeline consists of three main stages: encoding of EEG and music signals into latent representations, alignment of the two modalities in a shared embedding space, and decoding for music reconstruction. On the music side, we adopt standard components, using the pretrained CLAP audio encoder [31, 14] to obtain semantic audio embeddings, and a pretrained AudioLDM decoder [14] for music generation. Alignment is performed using a CLIP-style contrastive learning framework. Our primary contribution lies in the EEG representation and its integration with alignment. We introduce a channel-oriented design with three key components: channel-wise tokenization and channel-wise multi-view self-distillation, which are applied during the EEG encoding stage to preserve and aggregate weak, distributed neural signals, and channel-wise data augmentation, which is applied during the alignment stage to improve robustness. Figure 1 provides an overview of the main architecture of our pipeline.

3.1 Channel-wise Tokenization, Multi-view Self-distillation, and Data Augmentation

Channel-wise tokenization. First, we propose a transformer-based encoder that treats each channel as a first-class unit. Instead of forming tokens from spatial channel groups or applying early channel mixing, we construct tokens separately within each channel and let the transformer learn cross-channel interactions afterward. This design preserves the spatial origin of each measurement while still allowing global attention to combine evidence across electrodes, retaining both channel identity and temporal structure.

Specifically, each trial is divided into temporal windows of length t and stride s . At the 125 Hz sampling rate, each window contains $125t$ time samples. Within a window, every electrode signal is partitioned into temporal patches with positional embeddings. The transformer then attends over the resulting channel time tokens and produces $n + 1$ latent tokens, where the additional token is the CLS representation used for downstream alignment.

Channel-wise multi-view self-distillation. Next, we propose to pretrain the channel-oriented encoder using a DINO-style multi-view self-distillation objective [3] before any paired EEG-music training. This design enforces consistency across temporal scales and observed electrode subsets. Crucially, electrode identity remains explicit through channel tokens, while the pretraining objective encourages the representation to remain stable under missing or noisy channels, thereby improving robustness prior to alignment.

Specifically, each EEG segment is projected into a latent space and augmented into multiple temporal views: global views are large crops spanning 50-90% of the time series, and local views are smaller crops spanning 10-50%. The teacher processes only global views, while the student processes both global and local views under random channel dropout, so they often observe different channel subsets. Both share the same channel-oriented encoder and projection head. The student is trained to match the teacher’s output distribution via cross-entropy, with the teacher updated as an exponential moving average of the student. Each teacher output is matched with all student views of the same segment, which enforces consistency across temporal scales and channel subsets, and encourages the model to aggregate information across electrodes and to distinguish stable stimulus-related structure from channel-specific noise. Algorithm 1 outlines the main steps of channel-wise multi-view self-distillation.

Algorithm 1 Channel-wise multi-view self-distillation.

```

1: Input: EEG dataset  $\mathcal{D}$ 
2: Initialize: student encoder  $\theta_s$ , teacher encoder  $\theta_t \leftarrow \theta_s$ 
3: while not converged do
4:   Sample mini-batch  $X$  from  $\mathcal{D}$ 
5:   Generate two global crops  $V_g$  and  $K$  local crops  $V_l$  for each  $x \in X$ 
6:    $Z_s \leftarrow \{f_{\theta_s}(v) \mid v \in V_g \cup V_l\}$  with channel dropout;  $Z_t \leftarrow \text{stopgrad}\{f_{\theta_t}(v) \mid v \in V_g\}$ 
7:    $\mathcal{L} \leftarrow \sum_{z_t \in Z_t} \sum_{z_s \in Z_s \setminus \{z_t\}} \text{CE}(z_t/\tau_t, z_s/\tau_s)$ 
8:    $\theta_s \leftarrow \theta_s - \eta \nabla_{\theta_s} \mathcal{L}$ ;  $\theta_t \leftarrow \lambda \theta_t + (1 - \lambda) \theta_s$ 
9: end while

```

Channel-wise data augmentation. Finally, we introduce structured channel dropout as a data augmentation strategy to improve diversity and robustness. During alignment training, both EEG and music signals undergo random resized cropping and Gaussian perturbation, while the EEG branch additionally applies channel dropout. Because each electrode is represented as an explicit token, dropping channels removes structured spatial measurements rather than arbitrary feature dimensions. This encourages the model to infer consistent music-aligned representations from varying electrode subsets, reducing reliance on any fixed montage and improving robustness to noise, subject variability, and local artifacts. Algorithm 2 outlines the EEG augmentation.

Algorithm 2 Channel-wise data augmentation.

```

Require: data  $x \in \mathbb{R}^{C \times L}$ , crop scale  $p$ , noise level  $\sigma$ 
Ensure: Augmented time series  $x' \in \mathbb{R}^{C' \times L}$ 
1:  $x \leftarrow \text{ChannelDrop}(x)$ 
2:  $L_c \leftarrow \lfloor pL \rfloor$ ,  $i \sim \mathcal{U}(0, L - L_c)$ 
3:  $\tilde{x} \leftarrow \text{Interpolate}(x[:, i:i+L_c], \text{size} = L)$ 
4: return  $x' \leftarrow \tilde{x} + \epsilon$ ,  $\epsilon \sim \mathcal{N}(0, \sigma^2 I)$ 

```

3.2 Music Encoder, Alignment, and Reconstruction

We integrate the proposed channel-oriented design into a complete EEG-to-music pipeline consisting of three stages: encoding, cross-modal alignment, and music reconstruction.

Music encoder. We adopt the pretrained CLAP audio encoder from AudioLDM [31, 14] to extract semantic music embeddings. Audio is segmented according to the EEG windows, encoded by frozen CLAP, and projected into the shared alignment space. Keeping CLAP frozen gives a stable target for EEG alignment and matches the conditioning space used by the downstream AudioLDM decoder.

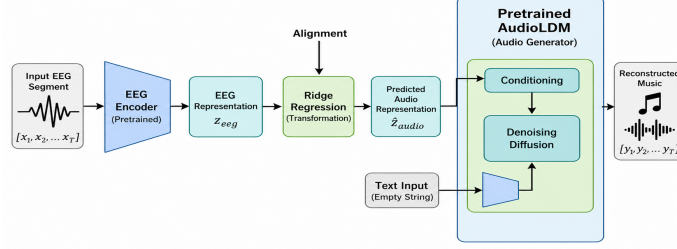


Figure 2: The reconstruction pipeline. After alignment, EEG representations are mapped to the CLAP audio embedding space using ridge regression. The transformed embedding is then used to condition AudioLDM for music reconstruction.

Alignment. Given pretrained EEG and audio encoders, we align the two modalities with a CLIP-style contrastive objective. EEG token embeddings are aggregated and projected through a temporal convolution followed by linear layers. For a batch of paired EEG and audio segments with batch size B and embedding dimension D , we obtain $Z_{eeeg} \in \mathbb{R}^{B \times D}$ and $Z_{audio} \in \mathbb{R}^{B \times D}$, and optimize a cross-entropy loss over the similarity matrix $Z_{eeeg} Z_{audio}^\top \in \mathbb{R}^{B \times B}$. This objective encourages matched EEG and audio pairs to be closer than mismatched pairs, while EEG channel dropout makes this alignment robust to missing or noisy electrodes.

Music decoder. To evaluate alignment quality and enable waveform reconstruction, we employ a pretrained diffusion-based audio generator, AudioLDM [14], without fine-tuning. A lightweight ridge regression adapter maps aligned EEG embeddings into the CLAP space expected by the decoder. At test time, the adapted EEG embedding conditions AudioLDM to generate audio. Because the generator is fixed and the adapter is linear, performance gains primarily reflect improvements in EEG representation and alignment, rather than decoder capacity. Figure 2 outlines this reconstruction pipeline.

4 Theoretical Analysis

We conduct a theoretical analysis of channel masking, through its induced augmentation graph, to provide a principled understanding of the proposed design. We begin by defining the augmentation kernel and a notion of normalized cross-cluster overlap. We then characterize the difference between channel-wise and block-wise masking through a simple reweighting identity in Lemma 4.1. Building on this result, we show that, under an interpretable covariance condition, channel-wise masking reduces cross-cluster overlap in Theorem 4.2. We give the proofs and additional discussions in Appendix A.

Let $\bar{x} \in \mathcal{X} \subseteq \mathbb{R}^N$ denote a channel-level representation of one EEG window, where N is the number of channel-level coordinates being masked. Let p denote the corresponding EEG data distribution. We write \mathcal{A} for a masking augmentation distribution, with \mathcal{A}_{cha} denoting channel-wise masking and \mathcal{A}_{blk} denoting block-wise masking. Let $y: \mathcal{X} \rightarrow \mathcal{Y}$ denote a discrete music-induced cluster label, such as an idealized song, genre, or semantic music cluster associated with an EEG window. Channel-wise masking samples each channel independently with retention probability ρ . Block masking partitions the channels into K disjoint blocks B_1, \dots, B_K , and samples one shared mask per block. For a pair (\bar{x}, \bar{x}') , let $D(\bar{x}, \bar{x}') = \{i \mid \bar{x}_i \neq \bar{x}'_i\}$, and $\mathcal{B}(D) = \{k \mid B_k \cap D \neq \emptyset\}$. Define $S(D) = |D| - |\mathcal{B}(D)| = \sum_k \max(0, |D \cap B_k| - 1)$. This quantity is large when the differences concentrate in a few blocks. Let $K_{\mathcal{A}}$ denote the augmentation overlap kernel induced by \mathcal{A} , and $\mathbf{1}[E]$ denote the indicator of an event E , which equals one when E is true and zero otherwise. We define the normalized cross cluster overlap as

$$r_y(\mathcal{A}) = \frac{\mathbb{E}_{p \otimes 2} [\mathbf{1}[y(\bar{x}) \neq y(\bar{x}')] K_{\mathcal{A}}(\bar{x}, \bar{x}')] }{\mathbb{E}_{p \otimes 2} [K_{\mathcal{A}}(\bar{x}, \bar{x}')]}. \quad (1)$$

A smaller value of r_y indicates that the augmentation graph places less mass across music-induced cluster boundaries.

The next lemma characterizes the difference between channel-wise and block-wise masking. Let $a = \rho^2 + (1 - \rho)^2$ and $b = (1 - \rho)^2 / a$. We note that the constant a^{N-K} cancels in r_y , while the only data-dependent term is $b^{S(D)}$, which downweights the pairs whose differences are concentrated in blocks.

Lemma 4.1 (Reweighting identity). *Under some standard masking assumptions given in Appendix A.1,*

$$\frac{K_{\text{cha}}(\bar{x}, \bar{x}')}{K_{\text{blk}}(\bar{x}, \bar{x}')} = a^{N-K} b^{S(D)}, \quad b \in (0, 1).$$

Let Q denote the probability measure on $\mathcal{X} \times \mathcal{X}$ with density proportional to $p(\bar{x})p(\bar{x}')K_{\text{blk}}(\bar{x}, \bar{x}')$, and write $Y(\bar{x}, \bar{x}') = \mathbf{1}[y(\bar{x}) \neq y(\bar{x}')]$. The next theorem shows that channel-wise masking yields strictly smaller normalized cross-cluster overlap than block masking.

Theorem 4.2 (Per-channel masking strictly reduces cross cluster overlap). *Suppose the following covariance condition holds:*

$$\text{Cov}_Q(Y, b^{S(D)}) < 0. \tag{2}$$

Then, $r_y(\mathcal{A}_{\text{cha}}) < r_y(\mathcal{A}_{\text{blk}})$.

We make some remarks. First, the covariance condition in (2) is a structural assumption, rather than a universal property of EEG. It describes a regime in which discriminative EEG variation is concentrated within anatomically or functionally related channel groups, so that block masking may jointly remove multiple informative channels, whereas per-channel masking can still preserve part of the signal. This assumption is biologically plausible, as music- and emotion-related EEG responses are often reported in coherent frontal, temporal, and parietal channel groups [20, 13, 19, 33, 8]. Next, our analysis adopts two simplifications. One concerns the difference set $D(\bar{x}, \bar{x}')$, which is defined on channel-level states and, for continuous EEG, should be interpreted through quantized, denoised, or tolerance-based similarity. The other concerns the mapping y , which is treated as a discrete music-induced cluster label, whereas the actual pipeline aligns EEG to continuous CLAP embeddings. This remains a reasonable coarse abstraction because song identity, genre, and semantic neighborhoods can be viewed as cluster-like summaries of the continuous audio embedding space. Finally, we do not view Theorem 4.2 as a rigorous guarantee for the full pipeline, but as a theoretical understanding supporting the proposed channel-oriented design.

5 Numerical Experiments

5.1 Datasets

We use the Naturalistic Music EEG Dataset Tempo version (NMED-T) [15] and the Hindi version (NMED-H) [11], two most commonly used benchmark datasets for EEG-to-music task. Both are collected and preprocessed under a common protocol, yielding 125-channel EEG signals at 150 Hz, band-pass filtered (0.3-50 Hz), with artifacts removed and per-channel z-score normalization applied. NMED-T includes 20 subjects listening to 10 pop songs (4-5 minutes each). NMED-H includes 48 subjects listening to 4 Indian pop songs. For NMED-H, there are augmented variants that expand the stimuli to 16 versions, though we use only the original and reverse versions to avoid data leakage. In total, the combined dataset contains 29.4 hours of recordings from 68 subjects. We perform experiments on the combined dataset using a random 95/5 split over EEG-music segments. We adopt a within-subject split, because subjects are not exposed to the same set of songs. A cross-subject split would otherwise confound subjects with songs. The alignment dimension is set to $D = 512$.

5.2 Baseline Methods and Evaluation Metrics

We compare with four groups of baseline methods.

Linear EEG Reference. We fit a linear ridge regression from raw EEG features to CLAP music embeddings and use the same AudioLDM reconstruction pipeline. This is a naive EEG-based reference method that isolates the contribution of learned EEG representations and alignment.

Audio Reconstruction Reference. We feed the ground-truth music directly into AudioLDM. This reference method measures the degradation introduced by the fixed generator without any EEG prediction, and therefore serves as an oracle-style upper bound for the reconstruction pipeline. Since it bypasses EEG decoding and uses the true audio, EEG-based methods are not expected to outperform it on semantic reconstruction or identification metrics.

EEG2Mel. EEG2Mel [18] is the closest existing method that directly maps EEG to mel spectrograms and tests whether explicit channel-oriented alignment improves semantic reconstruction. We follow the original settings in [18] to ensure a faithful reproduction of the method.

State-of-the-art EEG foundation models. We compare against LaBraM [10], EEGPT [26], and CBraMod [27], integrating each encoder into the same alignment and reconstruction pipeline so that differences primarily reflect EEG representations. These baseline methods incorporate related

elements, such as channel tokenization, multi-view pretraining, or large-scale pretraining, but none combines all components as our channel-oriented design. We do not include NeuroGPT, EEG-DINO, or EEGMamba in comparison, as they either lack publicly available pretrained weights or have been reported to underperform LaBraM. We also note that, although these foundation models have been pretrained on much larger EEG corpora for longer durations, scale alone does not guarantee better performance on our task. Prior work shows that large-scale pretraining can accelerate convergence, but not necessarily improve final task accuracy, especially under domain mismatch [9, 17]. In contrast, our encoder is pretrained only on the much smaller dataset NMED, but uses a self-distillation objective tailored to naturalistic music listening, together with channel-wise tokenization and dropout. This yields a more cost-effective pipeline that remains well adapted to the target alignment problem.

Evaluation Metrics. Our primary evaluation metrics include the 50-way identification task, the 14-way identification task, and the CLAP score. The first two identification tasks evaluate EEG-music alignment before waveform generation. In the 50-way task, each EEG embedding retrieves its paired music embedding from 50 song pieces using cosine similarity, providing a fine-grained test of discrimination. In the 14-way task, it follows a similar setup but over 14 entire songs, offering a simpler and more interpretable song-level measure. The CLAP score evaluates reconstructed audio by measuring cosine similarity between generated and ground-truth embeddings from a pretrained CLAP model, capturing semantic fidelity in the same representation space used by the decoder. Our secondary metric is 10-way song genre classification accuracy, which assesses whether reconstructed audio preserves broad musical style. While perceptually meaningful, it is less discriminative than identification tasks, as multiple songs may share the same genre. Finally, we also report SSIM and PSNR as reference spectrogram metrics. These pixel-level measures can favor smooth or spectrogram-like outputs without reflecting perceptual or semantic quality, and may penalize valid diffusion outputs with different local structures. Therefore, we report them only for completeness, but do not treat them as primary metrics.

5.3 Main Results

Table 1 reports the numerical results, and we make the following observations.

The main gain is the improved semantic reconstruction and EEG-music alignment. Among the EEG-based methods, our approach achieves the best CLAP score, 10-way genre accuracy, 50-way identification, and 14-way identification. Because all learned EEG methods share the same ridge adapter and AudioLDM generator, these gains primarily reflect stronger EEG representations and a better-aligned EEG-music embedding space, rather than differences in decoder capacity. EEG2Mel performs poorly because it is trained to predict local mel spectrograms rather than to align EEG with semantic audio embeddings. This limitation is most evident in embedding-level identification, where success depends on capturing song-specific semantics rather than producing a locally plausible spectrogram.

The strongest evidence comes from embedding-level identification. The 50-way task is the most discriminative, requiring each EEG embedding to retrieve its paired music embedding from many candidates before waveform generation. Our model achieves 0.487, improving by 0.085 over CBraMod, the strongest foundation model baseline, and by 0.228 over EEG2Mel. The 14-way task is easier, where our score of 0.692 is comparable to CBraMod’s 0.690. Thus the 50-way result shows the clearest evidence that channel-oriented representations improve fine-grained EEG-music alignment.

Spectrogram metrics do not reliably reflect perceptual or semantic quality in this setting. EEG2Mel achieves higher SSIM and PSNR because it directly regresses mel spectrograms, yet it performs poorly on CLAP and the two identification tasks. Similar to our method, the oracle Audio

Table 1: Reconstruction and alignment evaluation with the benchmark NMED-T and NMED-H datasets.

| Role | Method | Audio-level ↑ | | | Embedding-level ↑ | | |
|------------|--------------------------------|---------------|-------|--------------|---------------------|---------------------|---------------------|
| | | SSIM | PSNR | CLAP | 10-way genre | 50-way id. | 14-way name |
| Reference | Linear EEG Reference | 0.491 | 14.32 | 0.576 | 0.126±0.067 | 0.018±0.057 | 0.067±0.057 |
| | Audio Reconstruction Reference | 0.416 | 13.26 | 0.752 | 0.276±0.060 | 0.598±0.069 | 0.775±0.061 |
| Comparison | EEG2Mel | 0.762 | 24.37 | 0.588 | 0.132±0.051 | 0.259±0.050 | 0.478±0.062 |
| | LaBraM [10] | 0.422 | 14.21 | 0.657 | 0.162±0.056 | 0.380±0.057 | 0.681±0.051 |
| | EEGPT [26] | 0.378 | 14.34 | 0.625 | 0.141±0.065 | 0.326±0.069 | 0.643±0.068 |
| | CBraMod [27] | 0.418 | 14.42 | 0.641 | 0.169±0.059 | 0.402±0.058 | 0.690±0.064 |
| Proposed | Ours | 0.488 | 14.41 | 0.683 | 0.203 ±0.055 | 0.487 ±0.067 | 0.692 ±0.062 |

Table 2: Ablation studies for isolating individual component effects of the channel-oriented design.

| Component | Variant | 50-way \uparrow | 14-way \uparrow |
|-------------------|---------------------------------|--------------------------|--------------------------|
| Full model | Ours | 0.487 \pm 0.053 | 0.692 \pm 0.067 |
| Tokenization | Block tokenization | 0.141 \pm 0.064 | 0.406 \pm 0.062 |
| Pretraining | No multi-view pretraining | 0.050 \pm 0.067 | 0.155 \pm 0.066 |
| Channel dropout | No channel dropout | 0.411 \pm 0.067 | 0.598 \pm 0.054 |
| Temporal modeling | Linear head, encoder fixed | 0.092 \pm 0.065 | 0.191 \pm 0.061 |
| | Linear head, encoder fine-tuned | 0.422 \pm 0.051 | 0.612 \pm 0.063 |
| | Encoder fixed during alignment | 0.179 \pm 0.062 | 0.425 \pm 0.063 |

Reconstruction Reference only yields modest SSIM and PSNR despite using ground-truth music as input. These results indicate that pixel-level spectrogram distances like SSIM and PSNR are not good indicators for diffusion-based audio reconstruction and should not be treated as primary metrics.

5.4 Ablation Study

Table 2 presents the ablation results, isolating each component of the channel-oriented design under the same data split and reconstruction pipeline as the full model. We report only the 50-way and 14-way identification metrics, as they directly assess EEG-music alignment before waveform generation. The full model serves as the reference, with scores of 0.487 and 0.692.

Channel-wise tokenization is the largest contributor. Replacing per-electrode tokens with block tokens that group $g = 5$ contiguous electrodes reduces performance from 0.487 to 0.141 on the 50-way task and from 0.692 to 0.406 on the 14-way task, the largest drop in the ablation study. This strongly supports the first component of the channel-oriented design: preserving electrode identity is far more effective than early mixing of nearby channels before the model learns which electrodes carry music-relevant information. It also aligns with Theorem 4.2, which predicts an advantage for channel-level masking when informative variation is distributed within coarse channel blocks.

Channel-wise self-distillation enables effective use of the token representation. Training the same encoder from random initialization reduces performance from 0.487 to 0.050 on the 50-way task and from 0.692 to 0.155 on the 14-way task, showing that channel-wise tokenization alone is insufficient. This supports the second component of the design: multi-view self-distillation learns stable temporal and cross-channel structure under varying temporal crops and channel subsets before paired EEG-music alignment. In this sense, tokenization provides the appropriate representation interface, while self-distillation learns how to aggregate and stabilize the distributed neural signals across channels.

Channel-wise augmentation enhances robustness to missing or incomplete signals. Removing channel dropout reduces performance from 0.487 to 0.411 on the 50-way task and from 0.692 to 0.598 on the 14-way task. Although smaller than the effects of tokenization and pretraining, the drop is consistent across both metrics. This supports the third component of the design: random channel masking encourages the model to rely on distributed evidence rather than a fixed subset of electrodes.

The alignment head and encoder adaptation support the three core components. The temporal modeling ablations show how channel-oriented EEG tokens should be mapped to the music embedding space. With a fixed encoder and a linear head, the performance is poor at 0.092 and 0.191. Fine-tuning the encoder with the same linear head improves results to 0.422 and 0.612, indicating the importance of adaptation during alignment, but still falls short of the full temporal head, which reaches 0.487 and 0.692. Freezing the encoder during alignment also degrades the performance, yielding 0.179 and 0.425. Overall, these results show that the channel-oriented components are most effective when the alignment stage can jointly adapt the encoder and capture temporal structure.

5.5 Interpretability Analysis

Channel-wise tokenization makes per-electrode importance directly interpretable through attention weights. Specifically, the attention from the CLS token to channel tokens in the final transformer layer provides a per-channel score, which we average over heads, time windows, and subjects to obtain song-level scalp maps. In contrast, coarse block tokens would mix channels with different functional roles, obscuring this resolution. Figure 3 reports the per-channel patterns.

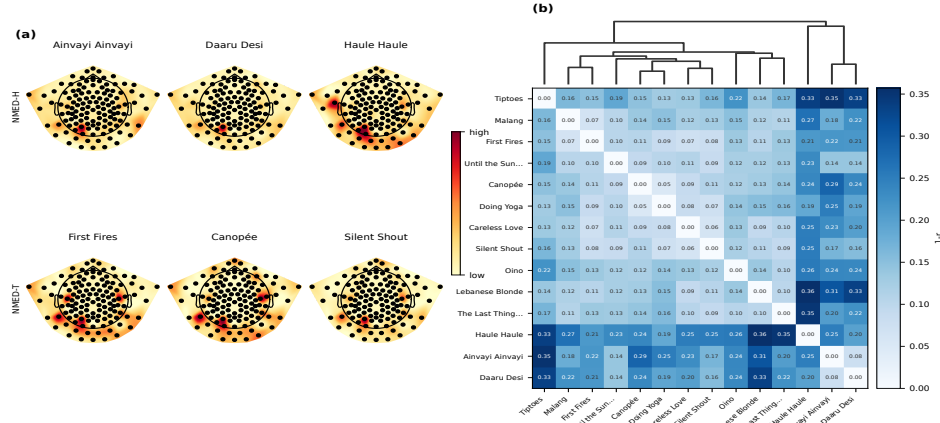


Figure 3: Channel attention patterns across songs. (a) Per-song maps for six representative songs from NMED-H (top) and NMED-T (bottom), plotted on the 10-10 scalp layout. (b) Pairwise dissimilarity between the 14 per-song maps as $1 - \text{Pearson correlation}$.

Posterior temporal attention reflects rhythmic auditory structure. Figure 3(a) shows the highest attention weights around lateral posterior temporal and temporo-occipital electrodes, with several songs exhibiting left-lateralized peaks rather than consistent right-hemisphere dominance. This pattern aligns with prior findings of bilateral auditory and superior temporal involvement during naturalistic music processing [12, 1]. The leftward peaks are also plausible, as alignment may rely on temporal features such as envelope, onset, and beat, particularly in the NMED-H stimuli, which contain strong rhythmic and percussive elements. Consistent with this, EEG responses to natural music track temporal structure and beat [11], and auditory temporal processing can show left-hemisphere preference [32]. As these maps reflect sensor-level attention rather than source-localized neural response, we interpret the lateralization cautiously as song-dependent posterior auditory involvement rather than definitive hemispheric specialization.

Dataset-level clustering reflects familiarity and enculturation effects. Figure 3(b) shows the dissimilarity matrix where the three NMED-H songs form a distinct cluster, with distances above 0.20 to most NMED-T songs, while many within-NMED-T distances remain between 0.05 and 0.15. NMED-H consists of Hindi pop and NMED-T of Western pop, with a largely Western listener pool in both datasets. This separation is consistent with findings that culturally unfamiliar music elicits different neural and behavioral responses [7], and that familiar music engages distinct neural processing [16]. These results suggest that the encoder captures stimulus features related to cultural familiarity beyond low-level acoustics.

6 Discussions

In this article, we show that improving EEG representation learning through channel-wise tokenization, self-distillation, and augmentation leads to much improved EEG-music alignment and semantic reconstruction. Our proposed channel-oriented design is both cost-effective and interpretable: it achieves strong performance with lightweight alignment and pretrained decoding components, while preserving per-channel representations that enable anatomically meaningful attention analysis. Together, the theoretical and empirical results support the central claim that representation design is crucial for decoding weak, distributed, and noisy EEG signals from music stimuli.

Limitations and Broader Impacts. The current study is limited by the size and scope of available EEG-music benchmark datasets, which contain only 29.4 hours of recordings and focus exclusively on music listening. Extending the framework to speech or environmental sounds would require larger paired datasets. The evaluation uses a within-subject split because NMED is not fully crossed across subjects and stimuli. Finally, the reconstruction stage intentionally uses a simple ridge adapter to isolate the effect of the proposed channel-oriented representation, while more expressive adapters and stronger music encoders remain important directions for future work. While our work may support assistive neurotechnology and the study of naturalistic perception, future applications should require informed consent, transparent data governance, and safeguards against covert or nonconsensual use.

References

- [1] Vinoos Alluri, Petri Toivainen, Iiro P Jääskeläinen, Enrico Glerean, Mikko Sams, and Elvira Brattico. Large-scale brain networks emerge from dynamic processing of musical timbre, key and rhythm. *NeuroImage*, 59(4):3677–3689, 2012.
- [2] Yunpeng Bai, Xintao Wang, Yan-Pei Cao, Yixiao Ge, Chun Yuan, and Ying Shan. Dreamdiffusion: High-quality eeg-to-image generation with temporal masked signal modeling and clip alignment. In *European Conference on Computer Vision*, pages 472–488. Springer, 2024.
- [3] Mathilde Caron, Hugo Touvron, Ishan Misra, Hervé Jégou, Julien Mairal, Piotr Bojanowski, and Armand Joulin. Emerging properties in self-supervised vision transformers. In *Proceedings of the IEEE/CVF international conference on computer vision*, pages 9650–9660, 2021.
- [4] Zijiao Chen, Jiabin Qing, Tiange Xiang, Wan Lin Yue, and Juan Helen Zhou. Seeing beyond the brain: Conditional diffusion model with sparse masked modeling for vision decoding. In *Proceedings of the IEEE/CVF Conference on Computer Vision and Pattern Recognition*, pages 22710–22720, 2023.
- [5] Zijiao Chen, Jiabin Qing, and Juan Helen Zhou. Cinematic mindscapes: High-quality video reconstruction from brain activity. *Advances in Neural Information Processing Systems*, 36: 24841–24858, 2023.
- [6] Wenhui Cui, Woojae Jeong, Philipp Thölke, Takfarinas Medani, Karim Jerbi, Anand A Joshi, and Richard M Leahy. Neuro-gpt: Towards a foundation model for eeg. In *2024 IEEE International Symposium on Biomedical Imaging (ISBI)*, pages 1–5. IEEE, 2024.
- [7] Steven M Demorest, Steven J Morrison, Münir Nuri Beken, and Daniel Jungbluth. Lost in translation: An enculturation effect in music memory performance. *Music Perception*, 25(3): 213–223, 2008.
- [8] Nikhil Garg, Rohit Garg, Apoorv Anand, and Veeky Baths. Decoding the neural signatures of valence and arousal from portable EEG headset. *Frontiers in Human Neuroscience*, 16:1051463, 2022. doi: 10.3389/fnhum.2022.1051463.
- [9] Kaiming He, Ross Girshick, and Piotr Dollár. Rethinking ImageNet pre-training. In *Proceedings of the IEEE/CVF International Conference on Computer Vision (ICCV)*, pages 4918–4927, 2019.
- [10] Wei-Bang Jiang, Li-Ming Zhao, and Bao-Liang Lu. Large brain model for learning generic representations with tremendous eeg data in bci. *arXiv preprint arXiv:2405.18765*, 2024.
- [11] Blair Kaneshiro, Duc T Nguyen, Anthony M Norcia, Jacek P Dmochowski, and Jonathan Berger. Natural music evokes correlated eeg responses reflecting temporal structure and beat. *NeuroImage*, 214:116559, 2020.
- [12] Stefan Koelsch. Brain correlates of music-evoked emotions. *Nature Reviews Neuroscience*, 15(3):170–180, 2014.
- [13] Yuan-Pin Lin, Jeng-Ren Duann, Jyh-Horng Chen, and Tzzy-Ping Jung. Electroencephalographic dynamics of musical emotion perception revealed by independent spectral components. *NeuroReport*, 21(6):410–415, 2010. doi: 10.1097/WNR.0b013e32833774de.
- [14] Haohe Liu, Zehua Chen, Yi Yuan, Xinhao Mei, Xubo Liu, Danilo Mandic, Wenwu Wang, and Mark D Plumbley. Audioldm: Text-to-audio generation with latent diffusion models. In *International Conference on Machine Learning*, pages 21450–21474. PMLR, 2023.
- [15] Steven Losorelli, Duc T Nguyen, Jacek P Dmochowski, and Blair Kaneshiro. Nmed-t: A tempo-focused dataset of cortical and behavioral responses to naturalistic music. In *ISMIR*, volume 3, page 5, 2017.
- [16] Carlos Silva Pereira, João Teixeira, Patrícia Figueiredo, João Xavier, São Luís Castro, and Elvira Brattico. Music and emotions in the brain: Familiarity matters. *PLoS ONE*, 6(11):e27241, 2011.
- [17] Maithra Raghu, Chiyuan Zhang, Jon Kleinberg, and Samy Bengio. Transfusion: Understanding transfer learning for medical imaging. In *Advances in Neural Information Processing Systems (NeurIPS)*, volume 32, 2019.

- [18] Adolfo G Ramirez-Aristizabal and Chris Kello. Eeg2mel: Reconstructing sound from brain responses to music. *arXiv preprint arXiv:2207.13845*, 2022.
- [19] Lars Rogenmoser, Nina Zollinger, Stefan Elmer, and Lutz Jäncke. Independent component processes underlying emotions during natural music listening. *Social Cognitive and Affective Neuroscience*, 11(9):1428–1439, 2016. doi: 10.1093/scan/nsw048.
- [20] Louis A. Schmidt and Laurel J. Trainor. Frontal brain electrical activity (EEG) distinguishes valence and intensity of musical emotions. *Cognition and Emotion*, 15(4):487–500, 2001. doi: 10.1080/02699930126048.
- [21] Paul S Scotti, Mihir Tripathy, Cesar Kadir Torrico Villanueva, Reese Kneeland, Tong Chen, Ashutosh Narang, Charan Santhirasegaran, Jonathan Xu, Thomas Naselaris, Kenneth A Norman, et al. Mindeye2: Shared-subject models enable fmri-to-image with 1 hour of data. *arXiv preprint arXiv:2403.11207*, 2024.
- [22] Yonghao Song, Bingchuan Liu, Xiang Li, Nanlin Shi, Yijun Wang, and Xiaorong Gao. Decoding natural images from eeg for object recognition. *arXiv preprint arXiv:2308.13234*, 2023.
- [23] Bob L Sturm. The gtzan dataset: Its contents, its faults, their effects on evaluation, and its future use. *arXiv preprint arXiv:1306.1461*, 2013.
- [24] Yu Takagi and Shinji Nishimoto. High-resolution image reconstruction with latent diffusion models from human brain activity. In *Proceedings of the IEEE/CVF conference on computer vision and pattern recognition*, pages 14453–14463, 2023.
- [25] Jerry Tang, Amanda LeBel, Shailee Jain, and Alexander G Huth. Semantic reconstruction of continuous language from non-invasive brain recordings. *Nature Neuroscience*, 26(5):858–866, 2023.
- [26] Guangyu Wang, Wenchao Liu, Yuhong He, Cong Xu, Lin Ma, and Haifeng Li. EEGPT: Pretrained transformer for universal and reliable representation of EEG signals. In *Advances in Neural Information Processing Systems (NeurIPS)*, 2024.
- [27] Jiquan Wang, Sha Zhao, Zhiling Luo, Yangxuan Zhou, Haiteng Jiang, Shijian Li, Tao Li, and Gang Pan. Cbramod: A criss-cross brain foundation model for eeg decoding. *arXiv preprint arXiv:2412.07236*, 2024.
- [28] Jiquan Wang, Sha Zhao, Zhiling Luo, Yangxuan Zhou, Shijian Li, and Gang Pan. Eegmamba: An eeg foundation model with mamba. *Neural Networks*, page 107816, 2025.
- [29] Jiquan Wang, Sha Zhao, Yangxuan Zhou, Yiming Kang, Shijian Li, and Gang Pan. Deeperbrain: A neuro-grounded eeg foundation model towards universal bci. *arXiv preprint arXiv:2601.06134*, 2026.
- [30] Xujia Wang, Xuhui Liu, Xi Liu, Qian Si, Zhaoliang Xu, Yang Li, and Xiantong Zhen. Eeg-dino: Learning eeg foundation models via hierarchical self-distillation. In *International Conference on Medical Image Computing and Computer-Assisted Intervention*, pages 196–205. Springer, 2025.
- [31] Yusong Wu, Ke Chen, Tianyu Zhang, Yuchen Hui, Taylor Berg-Kirkpatrick, and Shlomo Dubnov. Large-scale contrastive language-audio pretraining with feature fusion and keyword-to-caption augmentation. In *ICASSP 2023-2023 IEEE International Conference on Acoustics, Speech and Signal Processing (ICASSP)*, pages 1–5. IEEE, 2023.
- [32] Robert J Zatorre and Pascal Belin. Spectral and temporal processing in human auditory cortex. *Cerebral Cortex*, 11(10):946–953, 2001.
- [33] Jianhai Zhang, Ming Chen, Shaokai Zhao, Sanqing Hu, Zhiguo Shi, and Yu Cao. ReliefF-based EEG sensor selection methods for emotion recognition. *Sensors*, 16(10):1558, 2016. doi: 10.3390/s16101558.

A Proofs

A.1 Proof of Lemma 4.1

This lemma requires the following assumptions for masking-induced augmentation kernels, all of which are standard in the literature: (i) Each EEG window is represented by a channel-level vector $\bar{x} \in \mathcal{X} \subseteq \mathbb{R}^N$, and a masked view is $v = (M, M \odot \bar{x})$; (ii) The augmentation distribution factors as $\mathcal{A}(v | \bar{x}) = \pi(M) \delta(w - M \odot \bar{x})$ for $v = (M, w)$. Therefore two inputs overlap only when their retained coordinates agree; (iii) For channel-wise masking, the entries of M are independent Bernoulli(ρ) variables. For block-wise masking, the K block states are independent Bernoulli(ρ) variables and all coordinates in the same block share the same state; and (iv) The retention probability satisfies $0 < \rho < 1$, so the masking process is non-degenerate.

Proof. Let a view be $v = (M, M \odot \bar{x})$. The augmentation density factors as $\mathcal{A}(v | \bar{x}) = \pi(M) \delta(w - M \odot \bar{x})$ for $v = (M, w)$. Integrating over the view forces $w = M \odot \bar{x} = M \odot \bar{x}'$, which collapses to the indicator $\mathbf{1}[M_D(\bar{x}, \bar{x}') = 0]$. The remaining sum over M reads

$$K_{\mathcal{A}}(\bar{x}, \bar{x}') = \sum_M \pi(M)^2 \mathbf{1}[M_D = 0],$$

which is the overlap kernel used in the main text.

First, we consider the per-channel factorization. Under π_{cha} , the components of M are independent Bernoulli(ρ), so $\pi_{\text{cha}}(M)^2 = \prod_i \rho^{2M_i} (1-\rho)^{2(1-M_i)}$. The constraint $M_D = 0$ fixes $M_i = 0$ for every $i \in D$, and leaves M_i free for every $i \notin D$. Factoring across-channels gives

$$K_{\text{cha}}(\bar{x}, \bar{x}') = \prod_{i \in D} (1-\rho)^2 \cdot \prod_{i \notin D} (\rho^2 + (1-\rho)^2) = (1-\rho)^{2|D|} a^{N-|D|}.$$

Next, we consider block factorization. Under π_{blk} , mask states are constant within each block, and the K block states are independent Bernoulli(ρ). Writing $m_k \in \{0, 1\}$ for the state of block B_k , $\pi_{\text{blk}}(M)^2 = \prod_k \rho^{2m_k} (1-\rho)^{2(1-m_k)}$. The constraint $M_D = 0$ requires $m_k = 0$ for every $k \in \mathcal{B}(D)$, and leaves m_k free for every $k \notin \mathcal{B}(D)$. Factoring across blocks gives

$$K_{\text{blk}}(\bar{x}, \bar{x}') = \prod_{k \in \mathcal{B}(D)} (1-\rho)^2 \cdot \prod_{k \notin \mathcal{B}(D)} (\rho^2 + (1-\rho)^2) = (1-\rho)^{2|\mathcal{B}(D)|} a^{K-|\mathcal{B}(D)|}.$$

Finally, we obtain the result about the ratio. Dividing the two expressions and using $|D| - |\mathcal{B}(D)| = S(D)$ gives,

$$\begin{aligned} \frac{K_{\text{cha}}(\bar{x}, \bar{x}')}{K_{\text{blk}}(\bar{x}, \bar{x}')} &= (1-\rho)^{2(|D|-|\mathcal{B}(D)|)} a^{(N-|D|)-(K-|\mathcal{B}(D)|)} = (1-\rho)^{2S(D)} a^{(N-K)-S(D)} \\ &= a^{N-K} \left(\frac{(1-\rho)^2}{a} \right)^{S(D)} = a^{N-K} b^{S(D)}. \end{aligned}$$

Since $0 < \rho < 1$, we have $(1-\rho)^2 < \rho^2 + (1-\rho)^2 = a$, so $b = (1-\rho)^2/a \in (0, 1)$. \square

A.2 Proof of Theorem 4.2

Proof. Let $\Psi_y(\mathcal{A}) = \mathbb{E}_{p^{\otimes 2}}[Y K_{\mathcal{A}}]$ and $Z(\mathcal{A}) = \mathbb{E}_{p^{\otimes 2}}[K_{\mathcal{A}}]$. Then $r_y(\mathcal{A}) = \Psi_y(\mathcal{A})/Z(\mathcal{A})$.

By Lemma 4.1, $K_{\text{cha}}(\bar{x}, \bar{x}') = a^{N-K} K_{\text{blk}}(\bar{x}, \bar{x}') b^{S(D)}$ pointwise. The constant a^{N-K} pulls out of every expectation and appears identically in $\Psi_y(\mathcal{A}_{\text{cha}})$ and $Z(\mathcal{A}_{\text{cha}})$, so it cancels in $r_y(\mathcal{A}_{\text{cha}})$. Hence,

$$r_y(\mathcal{A}_{\text{cha}}) = \frac{\mathbb{E}_{p^{\otimes 2}}[Y K_{\text{blk}} b^S]}{\mathbb{E}_{p^{\otimes 2}}[K_{\text{blk}} b^S]} = \frac{\mathbb{E}_Q[Y b^S]}{\mathbb{E}_Q[b^S]},$$

where Q is the probability measure on $\mathcal{X} \times \mathcal{X}$ with density proportional to $p(\bar{x})p(\bar{x}')K_{\text{blk}}(\bar{x}, \bar{x}')$. Similarly,

$$r_y(\mathcal{A}_{\text{blk}}) = \frac{\mathbb{E}_{p^{\otimes 2}}[Y K_{\text{blk}}]}{\mathbb{E}_{p^{\otimes 2}}[K_{\text{blk}}]} = \mathbb{E}_Q[Y].$$

The difference is

$$r_y(\mathcal{A}_{\text{cha}}) - r_y(\mathcal{A}_{\text{blk}}) = \frac{\mathbb{E}_Q[Y b^S] - \mathbb{E}_Q[Y] \mathbb{E}_Q[b^S]}{\mathbb{E}_Q[b^S]} = \frac{\text{Cov}_Q(Y, b^S)}{\mathbb{E}_Q[b^S]}.$$

Because $b \in (0, 1)$ and $S(D) \geq 0$, $b^{S(D)} \in (0, 1]$ and $\mathbb{E}_Q[b^S] > 0$. Therefore, $r_y(\mathcal{A}_{\text{cha}}) < r_y(\mathcal{A}_{\text{blk}})$ holds if and only if $\text{Cov}_Q(Y, b^S) < 0$, which is exactly (2). \square

B More Details on Numerical Experiments

B.1 Benchmark Data, Code and Licenses

Our code will be publicly available upon publication, and generated music samples can be found at <https://eegmusic626-design.github.io/eegmusic/>. The code and data used for the reconstruction component are publicly available at <https://github.com/haoheLiu/AudioLDM>. AudioLDM is released under the Creative Commons Attribution NonCommercial ShareAlike 4.0 license. The NMED datasets and pretrained models used in this work are cited in the main text, and our use follows their public research terms.

B.2 Evaluation Protocol

Data split and windowing. For pretraining, EEG is downsampled to 125 Hz and segmented with an 8-second window and a 6.4-second stride, giving 1000 samples per window and 800 samples per stride. Eight local views and two global views are used. For alignment, we use a 1-second window and a 1-second stride. We randomly split EEG-music segments into 95% training and 5% testing sets.

Audio-level metrics. SSIM and PSNR measure mel spectrogram distance between reconstructed and groundtruth music. They are unreliable as primary metrics because diffusion-based generation can preserve perceptual content while changing phase, fine timing, or local spectral texture. Conversely, smoothed spectrogram predictions can score well while sounding less faithful. We therefore gray out these metrics in Table 1. The CLAP score is computed as cosine similarity between the reconstructed and ground-truth audio embeddings from a pretrained CLAP model [31]. The 10-way genre identification task uses a pretrained classifier with blues, classical, country, disco, hip hop, jazz, metal, pop, reggae, and rock genres [23].

Embedding-level metrics. For 50-way identification, we sample 50 paired EEG-music embeddings, compute the EEG-music cosine similarity matrix in the alignment space, and count whether each EEG embedding has the largest similarity with its paired music embedding. The 14-way identification task uses the same rule, with batches formed from 14 different songs. Both tests are repeated 10 times.

B.3 Baseline Method Implementations

Shared alignment protocol for foundation-model baselines. For LaBraM, EEGPT, and CBraMod, we replace only the EEG encoder while keeping the rest of the alignment and reconstruction pipeline fixed. Each EEG backbone output is passed through the same lightweight alignment head consisting of a linear layer with GELU activation, a linear projection into the shared alignment space, and layer normalization. The audio encoder remains frozen throughout training. EEG and audio embeddings are ℓ_2 normalized and optimized with a symmetric CLIP-style cross-entropy loss using a learned logit scale initialized at $\log(1/0.07)$. Unless otherwise stated, pretrained EEG backbones are initialized from the publicly released checkpoints and fine-tuned during alignment. All baselines are trained using the same optimization setup as our method, including AdamW, cosine learning-rate decay with warmup, gradient clipping, mixed precision training, and channel dropout augmentation.

EEG2Mel. We implement EEG2Mel [18] as the direct EEG-to-mel reconstruction baseline, following its original design of predicting mel spectrograms from EEG prior to waveform reconstruction. The input is an EEG PSD tensor of shape 63×125 , and the target is a 64×32 mel spectrogram. The network consists of five convolutional blocks with output channels 8, 16, 32, 64, 128, kernel size 4, ReLU activations, batch normalization, and dropout in the first four blocks. The resulting representation is max-pooled, flattened, and passed through two 128-dimensional fully connected layers before the final mel-spectrogram regression layer. Training uses mean-squared error on normalized mel spectrograms. For waveform reconstruction, the predicted mel spectrogram is clamped to $[-1, 1]$, rescaled to the original decibel range $[-70, 14]$, converted to a linear spectrogram via the inverse mel transform with 64 mel bins at a 16 kHz sampling rate, and synthesized using Griffin-Lim. The generated audio is evaluated using the same metrics as all other methods in Table 1.

LaBraM. For LaBraM [10], we use the official NeuralTransformer backbone from the fine-tuning implementation and initialize it with the publicly released checkpoint. The backbone uses a patch size of 200, embedding dimension 200, 12 transformer layers, 10 attention heads, MLP ratio 4, drop-path rate 0.1, and mean pooling. Since NMED EEG windows contain 125 channels, we pass the full 125-channel montage through the LaBraM channel-index interface. Because the alignment windows are shorter than the LaBraM patch size, the time dimension is zero-padded to the nearest patch multiple, scaled by $1/100$, and reshaped into channel-by-patch tensors before being fed into the backbone. We

discard the class token, average the remaining patch tokens, and pass the resulting representation to the shared alignment head.

EEGPT. For EEGPT [26], we use the official EEGPTClassifier backbone from the downstream EEGPT implementation and initialize it with the publicly released 58-channel, 4-second EEGPT checkpoint. The model is configured with input size 58×1024 , patch stride 64, the official 58-channel name list, mean pooling, channel-convolution adaptation enabled, and no predictor or output-projection head. Since the NMED recordings contain 125 channels, the channel-convolution front end is used to map the input into the pretrained EEGPT channel space. Short alignment windows are temporally adapted to the 1024-sample input length expected by the pretrained model. The resulting 512-dimensional EEGPT representation is then passed to the shared alignment head.

CBraMod. For CBraMod [27], we use the official implementation and initialize it with the publicly released pretrained weights. The backbone is configured with patch size 200, four temporal patches, model dimension 200, feed-forward dimension 800, 12 transformer layers, and 8 attention heads. Since CBraMod expects 22 EEG channels while NMED contains 125 channels, we learn a 1×1 convolutional channel adapter to map the 125-channel input into the pretrained channel space. The time dimension is interpolated to 800 samples when necessary and reshaped into four 200-sample patches. We remove the original output projection, average the backbone features across channel and patch dimensions, and pass the pooled representation to the shared alignment head. Because the CBraMod patch embedding includes an FFT operation that is not reliably supported in bfloat16 on common accelerators, the FFT path is computed in float32 before casting back prior to the alignment head.

B.4 Hyperparameters

The hyperparameters for pretraining and alignment are given in Tables 3 and 4. The reconstruction step is based on the AudioLDM [14] available at <https://github.com/haoheliu/AudioLDM>, with the sampling step set as 100.

Table 3: Encoder architecture and pretraining configuration. The left block lists the architecture and channel-oriented design parameters. The right block lists the multi-view self-distillation pretraining hyperparameters.

| Architecture | | Pretraining | |
|-----------------|-------|------------------------|-------------|
| Parameter | Value | Parameter | Value |
| Embedding dim | 512 | Global views | 2 |
| Patch size | 50 | Local views | 8 |
| Num channels | 125 | Crop (global) | [0.5, 1.0] |
| Channel dropout | 0.2 | Crop (local) | [0.1, 0.5] |
| Aligned dim | 512 | Noise (global / local) | 0.01 / 0.03 |
| Num heads | 16 | Learning rate | 8e-5 |
| Num layers | 8 | LR scheduler | Cosine |
| Window size | 1000 | Warmup steps | 6000 |
| Window stride | 800 | Train steps | 30000 |
| | | Batch size | 60 |

Table 4: Alignment hyperparameters.

| Category | Hyperparameter | Value |
|----------------|--------------------------|------------|
| Data windowing | EEG window size | 125 |
| | EEG window stride | 125 |
| Optimization | Learning rate | 1.2e-4 |
| | LR scheduler | Cosine |
| | LR warmup steps | 8000 |
| | Max train steps | 30000 |
| | Max gradient norm | 1.0 |
| | Batch size (train / val) | 500 / 50 |
| Augmentation | Crop scale | [0.4, 1.0] |
| | Noise level | 0.05 |
| | Channel dropout | 0.2 |

B.5 Computation of per-channel scores

Each electrode is represented as a separate input token to the alignment encoder, which produces a CLS token alongside the channel tokens at every transformer layer. We extract the attention weights from the CLS query to the channel keys in the final layer, average them across the 16 attention heads, and then aggregate across time windows within each song. To reduce subject-specific offsets, each subject-level attention map is z-scored across electrodes before averaging across subjects. The resulting per-song attention vector is projected onto the standard 10-10 scalp layout for visualization. This procedure does not require post-hoc saliency analysis, since electrode importance is directly encoded in the attention weights over channel tokens.

B.6 Hardware and Computation Time

All experiments are performed on a NVIDIA RTX 6000 Ada GPU. The total GPU time for pretraining and alignment is about 20 hours.